Water Air Soil Pollut (2015) 226:375
DOI 10.1007/s11270-015-2583-3

Synthesis and Application of Modified Zero-Valent Iron Nanoparticles for Removal of Hexavalent Chromium from Wastewater

Dan-Lian Huang · Guo-Min Chen · Guang-Ming Zeng · Piao Xu · Ming Yan · Cui Lai · Chen Zhang · Ning-Jie Li · Min Cheng · Xiao-Xiao He · Yan He

Received: 14 May 2015 / Accepted: 14 August 2015

Abstract Zero-valent iron nanoparticles (nZVI) modified with sodium dodecyl sulfate (SDS) as an anionic surfactant were successfully synthesized and applied to Cr (VI) removal. The prepared nanoparticles were characterized by field emission scanning electron microscope (FSEM), energy-dispersive spectrometry (EDS), and Fourier transform infrared spectrophotometer (FT-IR). Meanwhile, the surface charges of the stabilized nanoparticles were also determined. In this study, the kinetics of particle aggregation and sedimentation were investigated. It was found that the modified nanoparticles had great stabilization. Effects of pH, contact time, dosage of nanoparticles, and initial Cr(VI) concentrations on removal efficiency of the heavy metal ions were investigated and optimized. The maximum removal efficiency of Cr(VI) was obtained at pH 3.0 and 25 °C, at the value of 98.919 %. Cr(VI) removal occurred fast, and achieved equilibrium after 120 min. The maximum removal capacity reached up to 253.68 mg g^{-1} dry nanoparticles at a 300-mg L^{-1} Cr(VI)-containing sample. Kinetics study showed a rapid removal dynamics fitting pseudo-second-order kinetic model. The equilibrium data was nicely fit to the Freundlich model and indicates the adsorption of Cr(VI) was highly favorable. The obtained results indicated that nZVI modified by SDS could be used as an efficient alternative for removal of heavy metals with enhanced removal capacity and application stability.

Keywords Adsorption · Cr(VI) · Zero-valent iron nanoparticle · Sodium dodecyl sulfate · Kinetic

D.-L. Huang (✉) · G.-M. Chen · G.-M. Zeng (✉) · P. Xu · M. Yan · C. Lai · C. Zhang · N.-J. Li · M. Cheng · X.-X. He · Y. He
College of Environmental Science and Engineering, Hunan University, Changsha, Hunan 410082, People's Republic of China
e-mail: huangdanlian@hnu.edu.cn
e-mail: zgming@hnu.edu.cn

D.-L. Huang · G.-M. Chen · G.-M. Zeng · P. Xu · M. Yan · C. Lai · C. Zhang · N.-J. Li · M. Cheng · X.-X. He · Y. He
Key Laboratory of Environmental Biology and Pollution Control, Hunan University, Ministry of Education, Changsha 410082, People's Republic of China

1 Introduction

Heavy metals pollution originating from anthropogenic activities have posed a potential threat to the ecological system and human health, and have gradually drawn a wide concern across the globe because of its increased discharge, acute toxicity, persistence, bioaccumulation, and biomagnification through food chains (Xu et al. 2012a, b). Cr(VI) is one of the major heavy metal contaminants and has a severe harmful impact on public health, which damages the gastrointestinal, respiratory, and immunological systems, as well as causes reproductive and developmental problems (Fang et al. 2011; NIH Washington 2007). Effective disposals of heavy metal-bearing wastewater tend to be urgently demand.

The traditional treatment processes of wastewater include photocatalytic oxidation, adsorption/separation processing, and bioremediation (Huang et al. 2006, 2008; Xu et al. 2012a, b). However, their applications have been restricted by many factors including processing efficiency, operational method, energy requirements, and economic benefit. Recently, nanomaterials (NMs) have been suggested as cost-effective, efficient, and environmental friendly alternative to existing materials, from the standpoints of both environmental remediation and resource conservation (Huang et al. 2008). Especially, zero-valent iron nanoparticles (nZVI) has attracted significant interest because of its high reactivity and larger surface area (Bokare et al. 2008; Li and Zhang 2006; Kanel et al. 2006; Efecan et al. 2009). However, it has been recognized that nZVI tends to rapidly agglomerate to form larger aggregates due to magnetic forces and van der Waals, causing them undeliverable to the targeted contaminated locations (He and Zhao 2005; He et al. 2007). Moreover, bare-nZVI rapidly reacts with the surrounding media (e.g., water or dissolved oxygen), leading to rapid loss in reactivity as well as mobility. Because of agglomeration and the outer iron oxide or hydroxide layer, nZVI particles become poorly transportable or deliverable or reactive, and thus, might not be effectively applied for in situ remediation (De Gennes 1987).

To control nanoparticle agglomeration and thereby render the reactive particles more mobile, various particle stabilizing strategies have been reported, including polymers, polyelectrolytes, and surfactants. It has been reported that surface-modified nZVI could be effective for the remediation of a variety of priority pollutants, including heavy metals, polychorinated biphenyls (PCBs), chorinated pesticides, nitro compounds, and nitrates from contaminated groundwater, as well as wastewater (O'Carroll et al. 2013). He and Zhao have employed a sodium carboxymethyl cellulose (CMC) and food-grade starch as preagglomeration modifiers and achieved highly dispersed nZVI (He and Zhao 2005, 2007). Mohan Basnet et al. (2013) has found improved bare-nZVI mobility when the particles was suspended in the solution including rhamnolipid biosurfactant and soy protein (Basnet et al. 2013).

We choose sodium dodecyl sulfate (SDS) as stabilizer to modify zero-valent iron nanoparticle based on the fact that the surfactant has great migration and dispersion. On the one hand, since the oxidized nZVI surface layer may inhibit further electron transfer from the Fe^0 core to Cr(VI) at later reaction times, SDS on the nZVI surface could inhibit further oxidized nZVI surface layer formation. And the self-inhibition of reaction can be overcome by modified nZVI with SDS to increase both the rate and extent of Cr(VI) removal by reductive precipitation (O'Carroll et al. 2013). On the other hand, according to molecular structural formula of SDS as shown in Fig. 1, the $-SO_3$ group could adsorb directly with Cr(VI) on the surface of SDS-nZVI. The reaction process could be justified by exchange reactions in solutions during adsorption as shown below (Adeli et al. 2012; White et al. 2009):

$$RSO_3H + Na^+ \rightarrow RSO_3Na + H^+ \quad (1)$$

$$nRSO_3Na + M^{n+} \rightarrow (RSO_3)_nM + nNa^+ \quad (2)$$

$$6RSO_3Na + Cr^{6+} \rightarrow (RSO_3)_6Cr + 6Na^+ \quad (3)$$

In our study, batch experiments were carried out to study the removal ability of Cr(VI) ions from aqueous solution. Various factors, such as pH, contact time, and initial Cr(VI) concentrations, were studied. The kinetic studies were conducted to provide insight into the removal of Cr(VI). Experimental equilibrium data on adsorption isotherms were fitted to the Langmuir and Freundlich equations to confirm the best favorable isotherm.

2 Materials and Methods

2.1 Materials

Sodium borohydride ($NaBH_4$), ferrous sulfate heptahydrate ($FeSO_4 \cdot 7H_2O$), ethanol (CH_3CH_2OH), sodium dodecyl sulfate (SDS), potassium dichromate ($K_2Cr_2O_7$), sodium hydroxide (NaOH), and hydrochloric acid (HCl) were purchased from Kermel Tianjin/China. All chemicals used in this study were of analytical grade or higher.

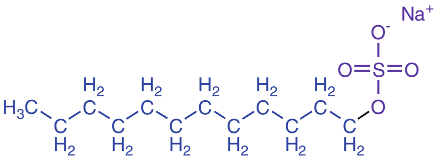

Fig. 1 Molecular structure of sodium dodecyl sulfate (*SDS*)

2.2 Preparation of Stabilized Nanoparticles

2.2.1 Preparation of Bare-nZVI

Zero-valent iron nanoparticles could be prepared in liquor solutions via the reduction of ferrous iron (Fe^{2+}) with sodium borohydride, which mechanism of preparation was showed as below:

$$Fe(HO)_6{}^{2+} + 2BH_4{}^{-} \rightarrow Fe^0\downarrow + 2B(OH)_3 + 7H_2\uparrow \quad (4)$$

Typically, 1:1 volume ratio of $NaBH_4$ (0.2 M) and FeSO4 (0.05 M) were vigorously mixed in the flask reactor (Sun et al. 2006; Yin et al. 2012). In brief, FeSO4 solution (preconditioned with N_2 sparging for deoxygenization) was poured in a 250-mL flask reactor, with N_2 simultaneous sparging and mechanical stirring. After NaBH4 was added, an additional 30 min of agitation was continued, ensuring the complete formation of homogeneous nZVI products. After complete precipitation and stratification, the final nanoparticles were washed three times with distilled water to eliminate free electrolyte. At last, the resultant products were collected by magnetic separating, and then freeze-dried for 24 h.

2.2.2 Preparation of SDS-nZVI Suspensions

The SDS-nZVI suspension was prepared by suspending the bare-nZVI particles into the SDS solution. The mixtures were sonicated for 40 min, operating at 20 kHz. Afterwards, complete precipitation and stratification by centrifuging at 5000 rpm for 5 min was performed, and then the supernatant was removed. Finally, we could separate SDS-nZVI by precipitation. The final nanoparticles were washed three times with distilled water to eliminate free SDS. Finally, the resultant products were collected by magnetic separating, and then freeze-dried for 24 h for further use. The schematic diagram of preparation of SDS-nZVI was shown in Fig. 2.

2.3 Characterization of Stabilized Nanoparticles

The surface morphological image and elemental composition were obtained from field emission scanning electron microscope (FSEM, JEOL JSM-7100F) and energy-dispersive spectrometry (EDS, EDAX genesis xm-2) after gold plating at an accelerating voltage of 20 kV. The corresponding Fourier transform infrared spectrophotometer (FT-IR) spectra of the nZVI were recorded on a Nicolet, Nexus-670 FT-IR spectrometer over the range of 4000~400 cm^{-1}. The surface charges of the stabilized nanoparticles were investigated by determining the point of zero charge (PZC) with a Zeta size Nano ZS.

2.4 Kinetics of Particle Aggregation and Sedimentation

2.4.1 Aggregation of Stabilized Nanoparticles

Aggregation of SDS-nZVI and bare-nZVI was investigated at a pH of around 8.5 with a batch test, by introducing different ionic strengths (NaCl) into the nanoparticles solutions (200 mg L^{-1}). The effect of Cl^{-} on nZVI oxidation was not considered in this study, given the fact of little effect on nZVI oxidation over 1 month of aging period in the presence of high concentration of Cl^{-} (10 mM) (Reinsch et al. 2010). Aggregation of the nanoparticles was monitored by measuring the average diameter via dynamic light scattering (DLS), according to the method described by Chen et al. (2007). The measurements were made at room temperature (25 °C), and all the experiments were carried out in triplicate.

2.4.2 Sedimentation of Stabilized Nanoparticles

In order to further investigate the stability of SDS-nZVI and bare-nZVI suspensions, the sedimentation was studied in a batch test. Typically, different concentrations of nanoparticles was prepared containing 1 mM $NaHCO_3$ (provide a circum-consistent pH value around 8.5±0.5), and sonicated for 5 min. Sedimentation was determined by UV scanning (λ=508 nm), as described by Phenrat et al. (2007). The measurements were made at room temperature (25 °C), and all the experiments were carried out in triplicate.

2.5 Batch Studies of Cr(VI) Removal

The removal of Cr(VI) from the aqueous solution was tested under various experimental conditions, including SDS-nZVI dosages, initial Cr(VI) concentrations, and pH of aqueous solution. pH values were adjusted to a range of 2 to 7 with dilute HCl or NaOH solution (0.1 M). Batch experiments were carried out at 25 °C in conical flasks containing 50 mL of Cr(VI) solution with desirable concentrations. The mixtures were placed on a controlled crystal oscillator at 150 rpm for 180 min

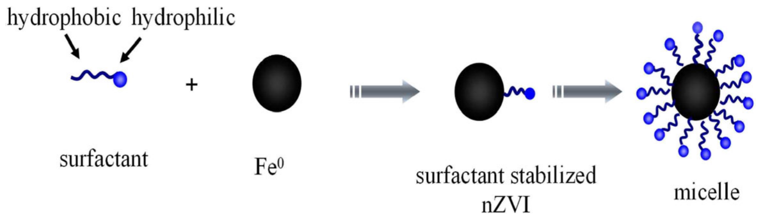

Fig. 2 Schematic diagram of the mechanism of nZVI stabilized by sodium dodecyl sulfate (*SDS*)

and then centrifuged at 5000 rpm for 10 min. The supernatant was filtered with 0.45-μm hydrophilic membranes, and the residual Cr(VI) was then analyzed. Control tests were carried out under identical conditions, except that bare-nZVI solution was used instead of a SDS-nZVI solution. The removal efficiency was calculated by Eq. (5):

$$\text{Cr removal efficiency}(\%) = (1 - C/C_0) \times 100\% \quad (5)$$

where C was the concentration of Cr(VI) at the specific time (mg L^{-1}), C_0 was the initial concentration of Cr(VI) (mg L^{-1}). All the experiments were carried out in triplicate, and data presented were the mean values from these independent experiments.

2.6 Analytical Methods

The residual Cr(VI) was determined colorimetrically at 540 nm using the diphenylcarbazide (DPC) method with a detection limit of 5 μg L^{-1}. Sample, 1 mL, was mixed with 9 mL of 0.2 M H_2SO_4 in a 10-mL volumetric flask. Subsequently, 0.2 mL of freshly prepared 0.25 % (*w*/*v*) DPC in acetone was added to the volumetric flask. After vortexing the mixture for about 15~30 s, it was allowed to stand for 10~15 min so as to ensure full color development. Using distilled water as reference, the red-violet to purple color formed was then measured at λ_{540} (Wang et al. 2014). The equilibrium concentration of total Cr (Cr_{total}) was measured by an atomic absorption spectrometer (AAS, Agilent 3510, USA).

3 Results and Discussion

3.1 Characterization of the Novel Modified Zero-Valent Iron Nanoparticles

3.1.1 FSEM Analysis of SDS-nZVI Particles

In order to observe the shape and size of the nanoparticles, FSEM studies were conducted and the FSEM images of bare-nZVI and SDS-nZVI were shown in Fig. 3. Figure 3a showed that the resulting bare particles did not become discrete; rather, they formed much bulkier dendritic flocs with different optical density. Owing to the electrostatic forces between nanoparticles and smaller particles and their surface tension interactions, the size of some greater flocs might be larger than 1 μm (He and Zhao 2007; Sun et al. 2006; Yin et al. 2012). As a result, a poorer reactivity could be attributed to lower

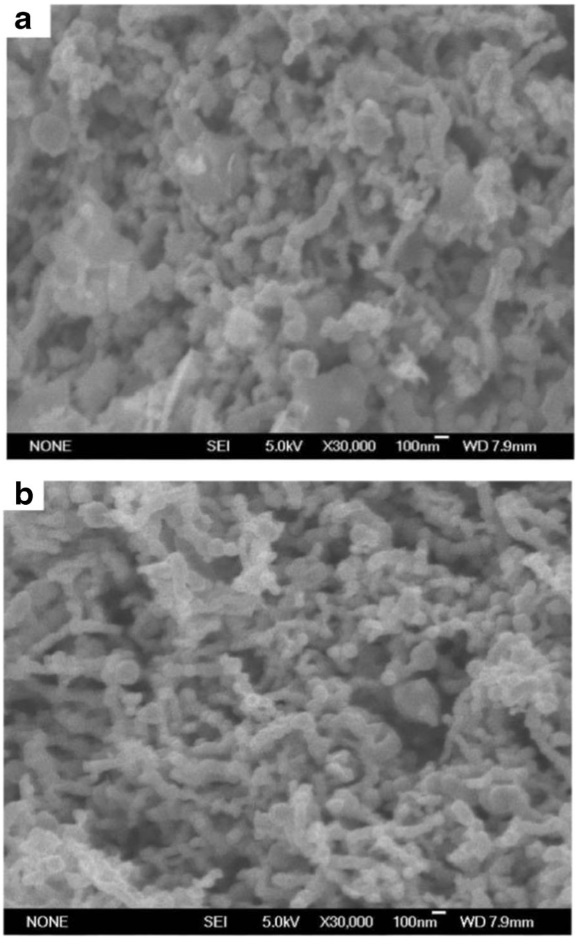

Fig. 3 FSEM images of the surface morphological for **a** bare-nZVI and **b** SDS-nZVI

surface area. In contrast, the SDS-nZVI presented in Fig. 3b was clearly discrete and well-dispersed, which was similar to spherical in shape. Additionally, it could be further confirmed by EDS analysis, as shown in Fig. 4. From Fig. 4a, it was found that the main elements were Fe and O. However, as demonstrated in Fig. 4b, in SDS-nZVI, the main elements of Fe, S, and O existed. And the elements of S and O accounted for a large proportion (10.78 and 38 %, respectively), which indicated that there were -SO_3 groups on the surface of nZVI. Therefore, the result indicated that nZVI had successfully modified with SDS.

3.1.2 FT-IR Spectra of SDS-nZVI

FT-IR measurements were carried out to confirm possible composition of synthesized nanoparticles. The spectrum for iron oxides (iron nanoparticles, maghemite, or pure Fe_2O_3) was characterized by a broad region composed of vibration bands at 724, 694, 632, 582, and 566 cm^{-1} (Veintemillas-Verdaguer et al. 1998; Wang and Ro 2007; Li et al. 2010). The main bands in the FT-IR spectrum of synthesized nZVI were showed in Fig. 5. It was showed that the Fe-O stretching bands appeared at 694.5 and 580.2 cm^{-1} in Fig. 5 line b, while the Fe-O stretching bands appeared at 586.6 cm^{-1} in Fig. 5 line a. What is more, it was shown that the S=O stretching bands presented at 1066 cm^{-1}, and the SO_3 stretching bands appeared at 1216 cm^{-1} (Zhang et al. 2006). This phenomenon illustrated that the surface modifier SDS had been coated on the surface of bare-nZVI.

3.1.3 Zeta Potential of SDS-nZVI

The zeta potential is a significant parameter that controls the interparticle electrostatic interactions and stability of nanoparticles in aqueous. Figure 6 showed the PZC of bare-nZVI and SDS-nZVI, where the SDS-nZVI carried a lower PZC than bare-nZVI. At neutral pH, the SDS-nZVI carried negative surface charges, while the bare-nZVI possessed a positive charge. In addition, the lowest PZC of SDS-nZVI could possibly be attributed to the adsorption of the surfactant with negative charges.

3.2 Kinetics of Particle Aggregation and Sedimentation

3.2.1 Aggregation of Stabilized Nanoparticles

It was found that the initial average particle sizes of bare-nZVI and SDS-nZVI were 220 and 300 nm, respectively (measured immediately after preparation). As shown in Fig. 7, with and without Na^+, both the bare-nZVI and SDS-nZVI tended to aggregate with time. However, the aggregation of bare-nZVI was more significant than the SDS-nZVI, which could be attributed to the following causes. On the one hand, due to initial smaller particle size, their surface energy increased (Li et al. 2006). Therefore, they tended to aggregate together to obtain stabilization. On the other hand, the zeta potential of bare-nZVI was lower than SDS-nZVI at a pH around 8 (Fig. 6), so that the electrostatic repulsion force among the nanoparticles was weaker for bare-nZVI leading to the aggregation among the nanoparticles. Because of the presence of SDS, the zeta potential of SDS-nZVI was more higher (Fig. 6), in which the electrostatic repulsion force among the nanoparticles was stronger. So, there was slight aggregation among SDS-nZVI. Moreover, it was found that the nanoparticles immediately aggregated with Na^+, at 30 min. But with time, there were no direct correlations to the aggregation. So, the reaction time had significant influence on aggregation of nanoparticles rather than the ionic strength.

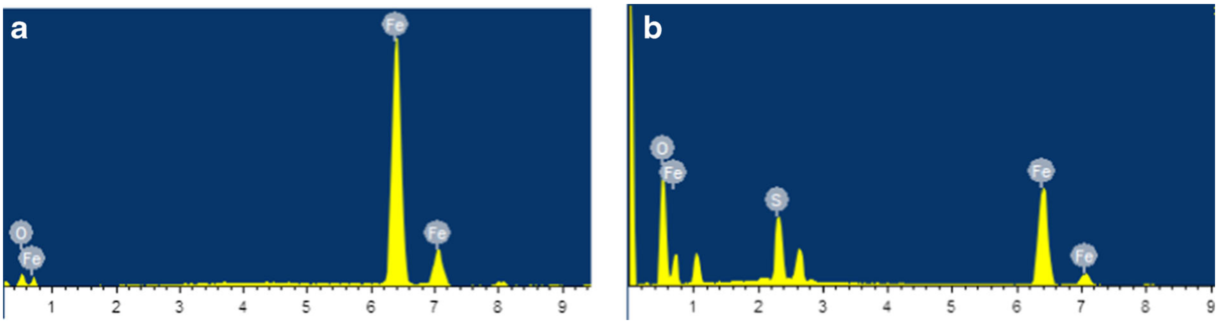

Fig. 4 EDS spectrum of stabilized nanoparticles. **a** Bare-nZVI. **b** SDS-nZVI

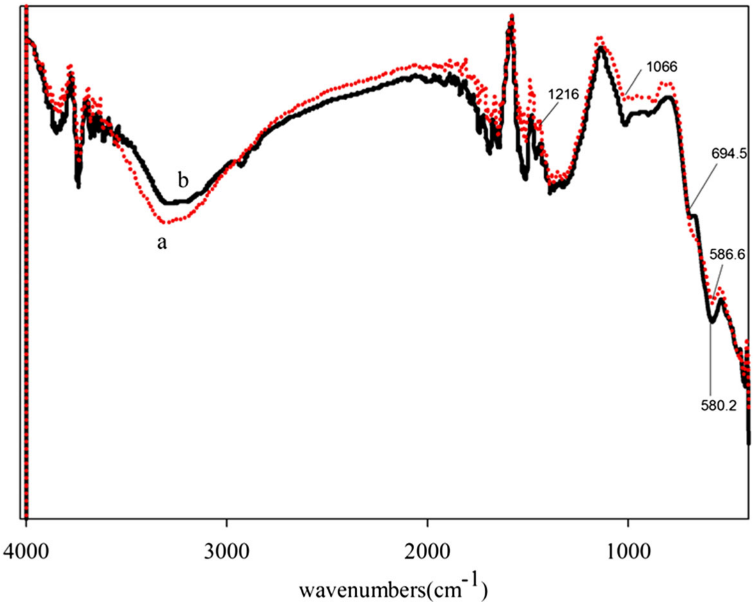

Fig. 5 FT-IR pattern of zero-valent iron nanoparticles (nZVI), **a** for the SDS-nZVI, and **b** for the bare-nZVI

3.2.2 Sedimentation of Stabilized Nanoparticles

Sedimentation kinetics of the bare-nZVI and SDS-nZVI were studied, and the results were shown in Fig. 8. The aggregation also could be affected by the concentration and zeta potential of the nanoparticles. As shown in Fig. 8, the lower the concentration of nanoparticles, the less sedimentation formed. This could be attributed to the difficulty of forming critical size chain-like clusters (Phenrat et al. 2007). Meanwhile, it was also found that bare-nZVI had more significant sedimentation than

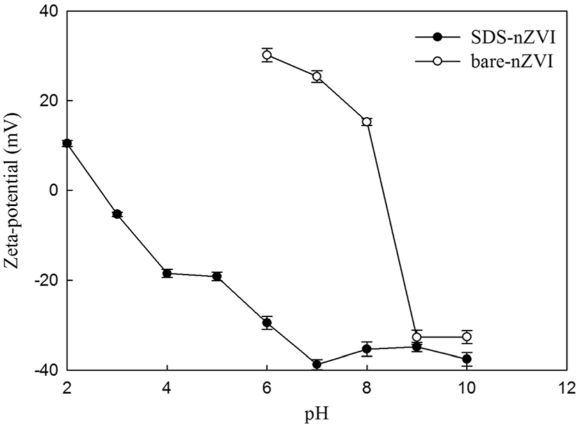

Fig. 6 The point of zero charge (*PZC*) of stabilized nanoparticles at pH range of 2–10

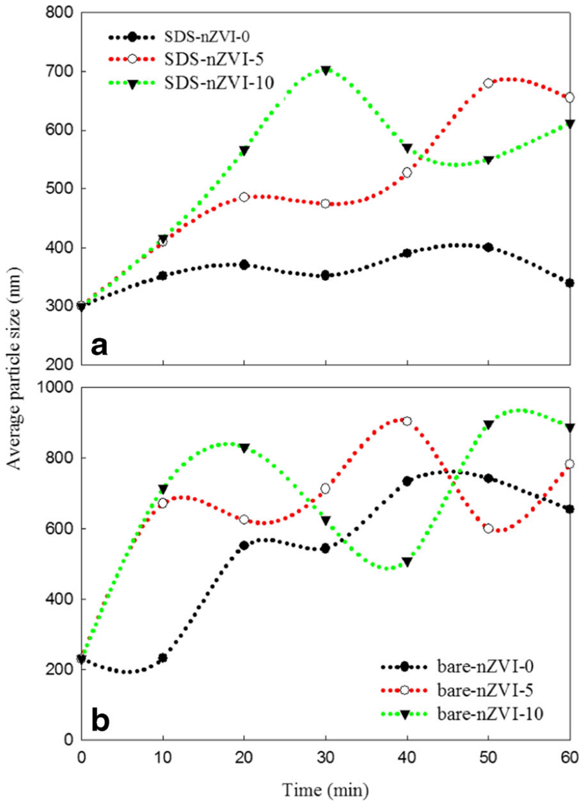

Fig. 7 Average particle size of nanoparticles (200 mg L^{-1}) under different ionic strengths (presented by varying NaCl concentrations, 5 and 10 mg L^{-1}) with time

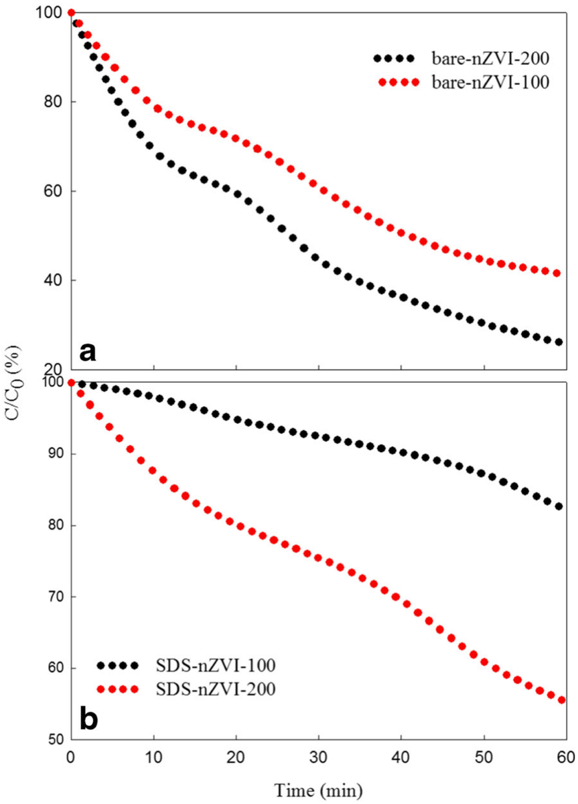

Fig. 8 Kinetics study of sedimentation of **a** bare-nZVI, **b** SDS-nZVI under different nanoparticles concentrations (100 and 200 mg L^{-1}) at pH around 8.5±0.5

SDS-nZVI with time, as shown in Fig. 8. The surface charge was almost neutral for bare-nZVI, and negative for SDS-nZVI at pH around 8 (Fig. 6). Therefore, because of the weaker electrostatic repulsion among bare-nZVI, the aggregation could occur more efficiently for bare-nZVI.

3.3 Effect of SDS on Cr(VI) Removal

In this study, SDS was added to the solution at concentrations lower than its critical micelle concentration (CMC (sodium carboxymethyl cellulose)=2.3 g L^{-1}) to modify the surface of nZVI (Hu et al. 2010). And the SDS/Fe^0 molar ratio ranges from 0.01:1 to 0.07:1. Figure 9 depicted that Cr(VI) removal efficiency increased as the amount of SDS added, while the removal efficiency decreased as the SDS/Fe^0 molar ratio was beyond 0.03:1. In the absence of SDS, the removal efficiency was close to 80 %. Such inefficiency of Cr(VI) removal might be ascribed to the agglomeration of bare-nZVI, which reduced the surface area and therefore the reactivity of nZVI (Wang et al. 2014; Lin and Juang 2002). In accordance with these results, the removal efficiency of Cr(VI) could be significantly increased with introducing SDS to modify the nanoparticles. And with the SDS/Fe^0 molar ratio below 0.05:1, removal efficiency of Cr(VI) grew remarkably as the SDS/Fe^0 molar ratio was increased. Maximum removal efficiency, closed to 98 %, was obtained as the SDS/Fe^0 molar ratio increased up to 0.03:1, whereas the removal efficiency decreased when the SDS/Fe^0 molar ratio was more than 0.05:1. Because SDS molecules began to form micelles in the bulk aqueous solution at higher concentrations; therefore, the SDS/Fe^0 molar ratio was 0.03:1 that the better stabilized nZVI was obtained.

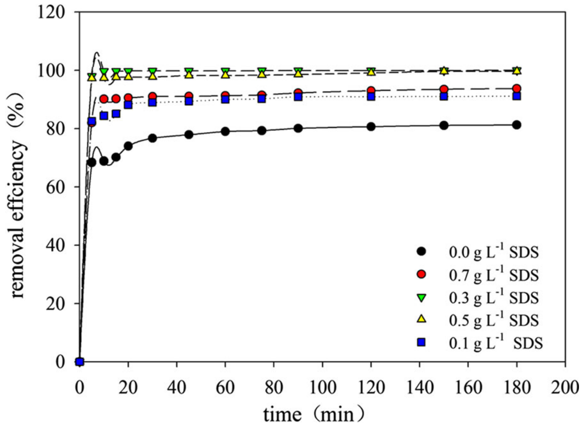

Fig. 9 Effect of SDS amount on the removal efficiency of Cr(VI). The sample volume of 50 mL with the initial Cr(VI) concentration of 50 mg L^{-1} at an initial pH of 4.5. The SDS concentration was adjusted to 0, 0.1, 0.3, 0.5, and 0.7 g L^{-1},,, respectively

3.4 Effect of pH on Cr(VI) Removal

The pH had significant influence on the metal ions removal from aqueous solutions. Metal sorption largely depended on pH, which has impacts both on the metal chemistry in solution and the ionization state of functional groups of the adsorbent, affecting the availability of binding sites (Heidari et al. 2009). The experiments were conducted in the pH range of 2~7 to assess the influence of pH on removal of Cr(VI). Figure 10 showed the Cr(VI) removal as a function of pH. It could be observed that the maximum removal efficiency of Cr(VI) by SDS-nZVI, at the value of 98.91 %, took place at around acidic pH=3. However, the removal efficiency of Cr(VI) by bare-nZVI was below 75 %. In contrast, it was found that the removal efficiency by SDS-nZVI decreased to 90.58 %, while pH>3. It might

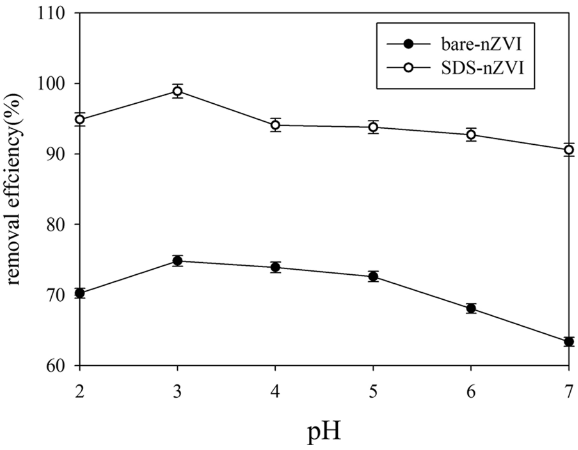

Fig. 10 Effect of pH on the removal efficiency of Cr(VI). The sample volume of 50 mL with the initial Cr(VI) concentration of 50 mg L^{-1}, at pH range of 2.0–7.0

be because mixed Fe and Cr oxyhydroxides were formed at high pH on nanoparticles surfaces, which caused that the surface was passivated and consequently lost the reactivity of the nanoparticles (Powell et al. 1995; Lee et al. 2003; Rivero-Huguet and Marshall 2009a, b). To achieve high extraction efficiency without metal hydroxide precipitation, pH of 3.0 for Cr(VI) was selected for subsequent experiments.

3.5 Effect of Contact Time on Cr(VI) Removal

The effect of contact time on the removal of Cr(VI) was illustrated in Fig. 11. It was observed that the removal efficiency increased with time. The removal process was rapid for the first 20 min as the removal efficiency increased from 0 to 95.77 %, followed by a slower speed. After 120 min, the reaction reached equilibration with a Cr(VI) removal efficiency of more than 96 %. Furthermore, the removal efficiency of Cr_{total} was up to 80 %. This result was attributed to the fast reduction of Cr(VI) by SDS-nZVI for the first 20 min, which could be explained by Eqs. (6) and (7). Additionally, with pH increased during the removal process, the products from the reduction of Cr(VI) were immobilized on the surface of SDS-nZVI, according to Eqs. (8) and (9). Therefore, the surface was covered by excess reaction products with time, leading to the removal of total Cr and the removal efficiency decreased and finally reached equilibration. This might serve as physical barriers, which prevented the electrons transporting from nZVI to Cr(VI). Reduction and co-precipitation were described below (Hou et al. 2008):

$$Cr_2O_7^{2-} + 3Fe^0 + 14H^+ \rightarrow 3Fe^{2+} + 2Cr^{3+} + 7H_2O \quad (6)$$

$$Cr_2O_7^{2-} + 6Fe^{2+} + 14H^+ \rightarrow 6Fe^{3+} + 2Cr^{3+} + 7H_2O \quad (7)$$

$$(1-x)Fe^{3+} + xCr^{3+} + 3H_2O \rightarrow (Cr_xFe_{1-x})(OH)_3\downarrow + 3H^+ \quad (8)$$

$$(1-x)Fe^{3+} + xCr^{3+} + 2H_2O \rightarrow Cr_xFe_{1-x}OOH\downarrow + 3H^+ \quad (9)$$

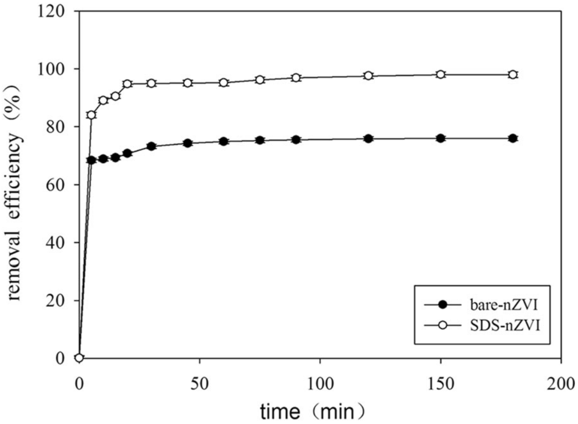

Fig. 11 Effect of time on the removal efficiency of Cr(VI). The initial Cr(VI) concentrations in all of the treatments were 50 mg L^{-1}. The sample volume of 50 mL using 1.0 g L^{-1} SDS-nZVI to react under different time at an initial pH of 3.0

3.6 Kinetics of Cr(VI) Removal

In order to evaluate the adsorption kinetics, the capacity of synthesized adsorbent was studied. Adsorption kinetic model was usually to estimated adsorption rate, and the mechanism of adsorption reactions could be better understood (Al-Degs et al. 2006). Two widely used models, pseudo-first-order and pseudo-second-order models, were used for experimental data to analyze kinetic.

3.6.1 Pseudo-First-Order Kinetic Model

The pseudo-first-order equation was expressed below (Li et al. 2009):

$$\ln(q_e - q_t) = \ln q_e + k_1 t \quad (10)$$

where k_1 is the rate constant of pseudo-first-order model (g mg^{-1} min^{-1}), t is the reaction time (min), q_t is the adsorption capacity at the specific time (mg g^{-1}), and q_e is the adsorption capacity at adsorption equilibrium (mg g^{-1}), respectively.

Figure 12a presented the results of pseudo-first-order kinetic model for experimental data. According to the plot of $\ln(q_e - q_t)$ vs t (Fig. 12), values of k_1 and q_e were calculated from the slope and intercept of the plot, and found in Table 1. It was found that a value for $k_1 < 1$ (Table 1) got closer to zero and varied in our study. Also, the linear correlation coefficient value (Table 1) was found to be the worst. It illustrated that description mass transfer resistance had no much influence on the adsorption rate. The results indicated that the pseudo-first-order kinetic model was not suitable for the removal of Cr(VI).

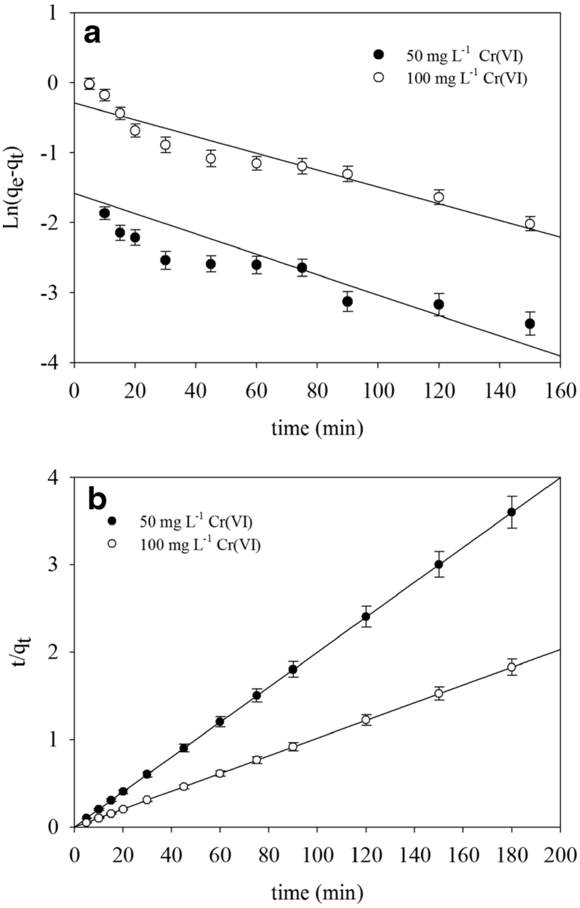

Fig. 12 Linear fit of experimental data for pseudo-first-order (**a**) and pseudo-second-order kinetic model (**b**) under various concentration of Cr(VI). The initial concentration of the Cr(VI) was 50, 100 mg L^{-1}

3.6.2 Pseudo-Second-Order Model

The rate of pseudo-second-order reaction might be related to the amount of metal ions adsorbed on the surface of nanoparticles and the amount adsorbed at equilibrium. With all in mind, the pseudo-second-order equation was expressed below (Yuan et al. 2010):

$$\frac{t}{q_t} = \frac{1}{k_2 {q_e}^2} + \frac{t}{q_e} \tag{11}$$

$$h = k_2 q_e^2 \tag{12}$$

where k_2 is the rate constant of pseudo-second-order model (g mg^{-1} min^{-1}), t is the reaction time (min), q_t is the adsorption capacity at the specific time (mg g^{-1}), and q_e is the adsorption capacity at adsorption equilibrium (mg g^{-1}), h (mg g^{-1} min^{-1}) is the initial sorption rate, respectively.

Fitting of kinetic data to the pseudo-second-order kinetic model was shown in Fig. 12b. Figure 12b presented favorable linear relation of the pseudo-second order model, and the correlation coefficients (R^2= 0.9999) was very high. This results revealed that this adsorption system fitted to the pseudo-second-order model, implying that the adsorption mechanism was related to solute and nanoparticles and it was the rate-limiting step that could be a chemical sorption including valence forces via sharing or exchanging of electrons (Xu et al. 2012a, b).

According to the plot of t/q_t vs t (Fig. 12), values of k_2 and q_e were calculated from the intercept and slope of the plot, and found in Table 1. It was observed that the values of calculated equilibrium capacities ($q_{e\ cal}$) from the pseudo-second-order and those of experimental capacities ($q_{e\ exp}$) at different initial Cr(VI) concentrations were almost accordant (see Table 1). The initial sorption rate h was 0.769 and 0.781 mg g^{-1} min^{-1}, respectively, at the concentration of 50 and 100 mg L^{-1} Cr(VI) ions. For any c_0 values within the scope of experiment, the initial adsorption rate h increased as the initial concentrations increase, implying that adsorption enhanced with the increased initial Cr(VI) concentration. The increase of initial adsorption rate might be attributed to a type of driving force supplied by the higher initial concentration, to overcome the existing mass transfer resistance of Cr(VI) between the liquor and solid phases (Xu et al. 2012a, b). Hence, the pseudo-second-order

Table 1 Kinetics constants for the adsorption of Cr(VI) at various concentrations

Pseudo-first-order model				Pseudo-second-order model			
c (mg L^{-1})	$q_{e\ exp}$(mg g^{-1})	K_1 (min^{-1})	R^2	$q_{e\ cal}$(mg g^{-1})	K_2 (mg mg^{-1} min^{-1})	h (mg g^{-1} min^{-1})	R^2
50	49.95	0.01457	0.5891	50	0.3077	0.769	0.9999
100	98.391	0.012101	0.9055	98.33	0.3125	0.781	0.9999

model greater represented the adsorption kinetics, which indicated that the removal of Cr(VI) with SDS-nZVI followed by chemisorption mechanism via electrostatic attraction, which was in accordance with the schematic diagram of prepared SDS-nZVI illustrated in Fig. 2, due to SDS, anionic surface active agent (Yuan et al. 2010; Jiang et al. 2013).

3.7 Effect of SDS-nZVI Dosages on Cr(VI) Removal

To estimate the optimum dose of SDS-nZVI, 0~0.075 g of freshly synthesized SDS-nZVI were added to 50 mL of Cr(VI)-containing solution at the concentration of 50 mg L^{-1}. Evidently, the removal efficiency was sensitive to the variation of SDS-nZVI content. Figure 13 illustrated an improvement of the concentration of Cr(VI) with the increasing in SDS-nZVI dose. This phenomenon might be contributed to that the increased dose of SDS-nZVI would provide more available reactive groups for metal binding on the surface of SDS-nZVI. Additionally, the increasing SDS-nZVI dose might have an impact on the concentration gradient of the surface of SDS-nZVI owing to the varying concentration of the solution (Boschi et al. 2011). Substantial dosage may provide more removal sites of SDS-nZVI and improve removal efficiency, but taking both the effectiveness and cost into consideration, the following experiments were conducted with a desired concentration of SDS-nZVI (1.0 g L^{-1}).

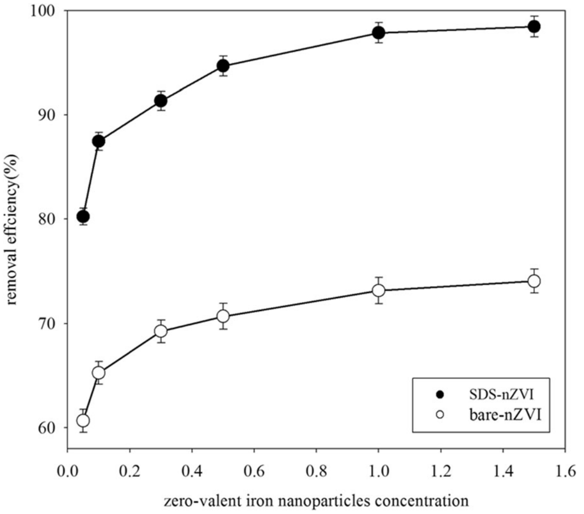

Fig. 13 Effect of SDS-nZVI dosages on the removal efficiency of Cr(VI). The sample volume of 50 mL with the initial Cr(VI) concentration of 50 mg/L at an initial pH of 3.0. The dosages of SDS-nZVI was adjusted to 0, 0.05, 0.1, 0.3, 0.5, 1.0, and 1.5 g L^{-1}, respectively

3.8 Effect of Initial Cr(VI) Concentration on Cr(VI) Removal

The removal capacity was found to be a function of the initial concentration of Cr(VI). To determine the removal ability, the experiments were carried out with the wide ranges of initial Cr(VI) concentration of 20~300 mg L^{-1}. The results, in terms of Cr(VI) removal efficiency and capacity versus initial concentration of Cr(VI), were presented in Fig. 14. It might be found that the removal efficiency reached approximately to 100 % with the increasing of Cr(VI) concentration below 80 mg L^{-1}. This phenomenon might be because the provided reactive sites were enough for the removal of all the Cr(VI) at low concentration. Furthermore, it had been illustrated that the initial concentration provided a type of significant driving force to overcome the existing mass transfer resistance of Cr(VI) ions between the aqueous and solid phases (Iram et al. 2010). However, the removal efficiency showed a declining trend while the Cr(VI) concentration was at high concentrations. It was likely that the insufficient available reactive sites on the surface of SDS-nZVI could result in a slowdown of Cr(VI) reduction. Additionally, as we expected, the whole trend of removal capacity increased as increasing initial concentrations of Cr(VI).

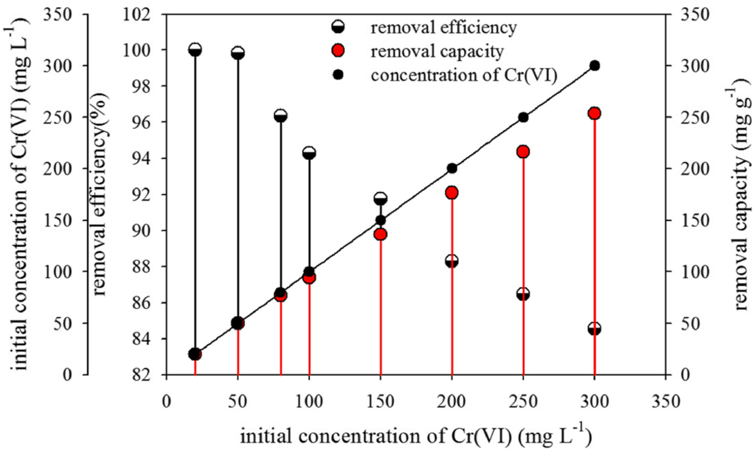

Fig. 14 Effect of initial concentration of Cr(VI) on the removal efficiency and capacity. The sample volume was 50 mL at an initial pH of 3.0. The dosages of SDS-nZVI in all of the treatments were 1.0 g L^{-1}, and the contact time was 120 min. The initial concentration of the Cr(VI) was 20, 50, 80, 100, 150, 200, 250, and 300 mg L^{-1}

3.9 Adsorption Isotherms

Adsorption isotherms aimed to explain the specific relation between the equilibrium concentration of solute in solution and adsorbed amount on surface. To measure the adsorption model of nanoparticles, isotherms studies were carried out with different initial Cr(VI) concentrations ranging from 20 to 300 mg L^{-1}, and analyzed by two adsorption isothermal models: Freundlich and Langmuir isotherm, at room temperature (298.15 K), as illustrated in Fig. 15. Maximum adsorption capacity was calculated to be 264.55 mg g^{-1} adsorbent at the initial concentration of 300 mg L^{-1}. Constants and correlation regression coefficients of Cr(VI) adsorption were presented in Table 2.

3.9.1 Langmuir Isotherm

The Langmuir isotherm was applied to evaluate the adsorption capacity of nanoparticles and suggested that uptake occurs on a homogeneous surface by monolayer sorption without interaction between adsorbed

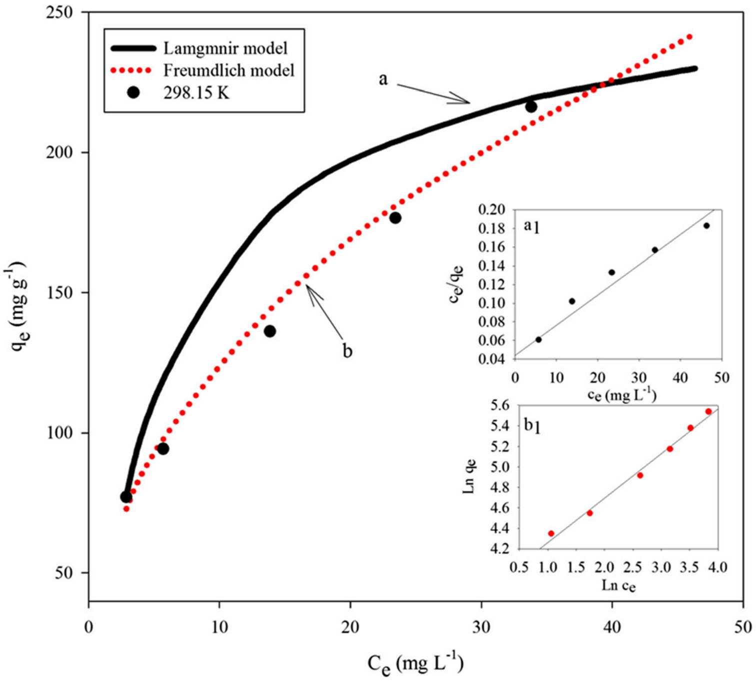

Fig. 15 Adsorption isotherms for Cr(VI) onto SDS-nZVI at 298.15 K with various concentrations. The initial concentration of the Cr(VI) was 50, 100 mg L^{-1}

Table 2 Isotherm constants for Cr(VI) adsorption onto SDS-nZVI at room temperature (298.15 K) with various concentrations

Freundlich model				Langmuir model			
T (K)	k_F	$1/n$	R^2	q_m (mg g^{-1})	k_L (L mg^{-1})	R_L	R^2
298.15	45.8236	0.04352	0.9906	264.55	0.1432	0.0227–0.2588	0.9320

molecules. The Langmuir model, supposing that adsorption took place at certain homogeneous sites, was applied to the data as the following equation (Langmuir 1916):

$$\frac{c_e}{q_e} = \frac{1}{q_m k_L} + \frac{c_e}{q_m} \tag{13}$$

where q_m is the maximum adsorption capacity (mg/g), k_L denotes the Langmuir constant (L mg^{-1}),,, and c_0 (mg L^{-1}) is the initial concentration of Cr(VI).

The linear plot of specific adsorption (c_e/qe) against the equilibrium concentration (c_e) showed that the sorption of Cr(VI) on SDS-nZVI obeyed the Langmuir model (R^2=0.9320) (Fig. 15a1). The Langmuir constants q_m and k_L were determined from the slope and intercept of the linear plot and were found to be 264.55 and 0.1432 L mg^{-1},,, respectively (Table 2).

The significant features of the Langmuir isotherm could be expressed as a dimensionless constant separation factor. R_L, which could be used to imply whether the adsorption model is favorable, was given by the following equation (Langmuir 1916):

$$R_L = \frac{1}{1 + K_L c_0} \tag{14}$$

where c_0 (mg L^{-1}) is initial concentration of adsorbent and K_L (L mg^{-1}) is the Langmuir constant. There are four probabilities for the R_L value: for favorable sorption, $0<R_L<1$; for unfavorable sorption, $R_L>1$; for linear sorption, $R_L=1$; and for irreversible sorption, $R_L=0$ (Hall et al. 1966). It was showed that the R_L values (Table 2) were varied from 0~1 at 25 °C, suggesting that the adsorption of Cr(VI) by SDS-nZVI was favorable. The R_L value was 0.0227, which indicated that the adsorption of Cr (VI) on SDS-nZVI was also favorable at high initial Cr(VI) concentration.

3.9.2 Freundlich Isotherm

Freundlich isotherm is widely applied, assuming that the binding sites on the surface of nanoparticles are heterogeneous, and the ratio of adsorbed solute to the solute concentration was a function of the solution (Gupta et al. 2010; Amin 2008). The Freundlich isotherm could be represented as:

$$\ln q_e = \ln\ k_F + \frac{1}{n} \ln\ c_e \tag{15}$$

where c_e is the equilibrium concentration of Cr(VI) (mg L^{-1}), and k_F and n are the Freundlich constants. k_F is defined as the adsorption coefficient (Gupta et al. 2010). Also, n is used to imply whether the sorption process is favorable.

According to the plot of lnq_e vs lnc_e (Fig. 15b1), values of k_F and n were calculated from the intercept and slope of the plot, and found to be 45.8236 and 2.2976 respectively (Table 2). Generally, $n<1$ demonstrated that sorption intensity was favorable over all range of concentrations, while $n>1$ revealed that sorption intensity was favorable at high concentrations rather than much less at lower concentrations (Al-Degs et al. 2006). In our study, n value was higher than 1, which suggested that sorption intensity was great over all concentrations and varied from 80 to 300 mg L^{-1}. A value for $1/n$ <1 indicated a normal Freundlich isotherm, becoming more heterogeneous as its value was much nearer to zero, while $1/n$ >1 was indicative of cooperative adsorption (Fytianos et al. 2000). In our study, the obtained $1/n$=0.43523 (Table 2) showed that the sorption process was heterogeneous.

4 Conclusion

In this work, zero-valent iron nanoparticles modified by SDS were successfully prepared and characterized by FSEM, EDS, and FT-IR. The kinetics of particle aggregation and sedimentation were investigated to evidence the stabilization of particles. It was found that aggregation was affected by the initial particle size and the zate potential, and sedimentation was related to the concentration and the zate potential of nanoparticles. It was found that the modified nanoparticles had great stabilization. The as-prepared SDS-nZVIs showed promising prospects for Cr(VI) removal. It was found that removal efficiency was dependent on experimental conditions. The optimal removal occurred at pH 3.0 and 25 °C with 1.0 g L^{-1} SDS-nZVI. In addition, the removal efficiency quickly increased at first 20 min, and then kept a continued increasing tendency at a slower rate, followed by an equilibrium period at 120 min. The adsorption followed the pseudo-second-order kinetic model, which showed higher correlation coefficients. This research provides compelling evidence that the stabilized ZVI nanoparticles may be used for the removal of Cr(VI) from wastewater, which may lead to an innovative treatment technology that is likely more cost-effective and less environmentally disruptive.

Acknowledgments The study was financially supported by the Program for the National Natural Science Foundation of China (51278176, 51408206, 51039001, 51378190), the Fundamental Research Funds for the Central Universities, Hunan University Fund for Multidisciplinary Developing (531107040762), the Program for New Century Excellent Talents in University (NCET-13-0186), the Hunan Provincial Innovation Foundation For Postgraduate (CX2013B152, CX2014B141), and the Program for Changjiang Scholars and Innovative Research Team in University (IRT-13R17).

References

Adeli, M., Yamini, Y., & Faraji, M. (2012). Removal of copper, nickel and zinc by sodium dodecyl sulphate coated magnetite nanoparticles from water and wastewater samples. *Arabian Journal of Chemistry.*

Al-Degs, Y. S., El-Barghouthi, M. I., Issa, A. A., Khraisheh, M. A., & Walker, G. M. (2006). Sorption of Zn (II), Pb (II), and Co (II) using natural sorbents: equilibrium and kinetic studies. *Water Research, 40*, 2645–2658.

Amin, N. K. (2008). Removal of reactive dye from aqueous solutions by adsorption onto activated carbons prepared from sugarcane bagasse pith. *Desalination, 223*, 152–161.

Basnet, M., Ghoshal, S., & Tufenkji, N. (2013). Rhamnolipid biosurfactant and soy protein act as effective stabilizers in the aggregation and transport of palladium-doped zerovalent iron nanoparticles in saturated porous media. *Environmental Science & Technology, 47*, 13355–13364.

Bokare, A. D., Chikate, R. C., Rode, C. V., & Paknikar, K. M. (2008). Iron-nickel bimetallic nanoparticles for reductive degradation of azo dye Orange G in aqueous solution. *Applied Catalysis B: Environmental, 79*, 270–278.

Boschi, C., Maldonado, H., Ly, M., & Guibal, E. (2011). Cd (II) biosorption using Lessonia kelps. *Journal of Colloid and Interface Science, 357*, 487–496.

Chen, K. L., Mylon, S. E., & Elimelech, M. (2007). Enhanced aggregation of alginate-coated iron oxide (hematite) nanoparticles in the presence of calcium, strontium, and barium cations. *Langmuir, 23*, 5920–5928.

De Gennes, P. G. (1987). Polymers at an interface; a simplified view. *Advances in Colloid and Interface Science, 27*(3), 189–209.

Efecan, N., Shahwan, T., Eroğlu, A. E., & Lieberwirth, I. (2009). Characterization of the uptake of aqueous Ni^{2+} ions on nanoparticles of zero-valent iron (nZVI). *Desalination, 249*, 1048–1054.

Fang, Z., Qiu, X., Huang, R., Qiu, X., & Li, M. (2011). Removal of chromium in electroplating wastewater by nanoscale zero-valent metal with synergistic effect of reduction and immobilization. *Desalination, 280*, 224–231.

Fytianos, K., Voudrias, E., & Kokkalis, E. (2000). Sorption–desorption behaviour of 2,4-dichlorophenol by marine sediments. *Chemosphere, 40*, 3–6.

Gupta, V. K., Rastogi, A., & Nayak, A. (2010). Biosorption of nickel onto treated alga (Oedogonium hatei): application of isotherm and kinetic models. *Journal of Colloid and Interface Science, 342*, 533–539.

Hall, K. R., Eagleton, L. C., Acrivos, A., & Vermeulen, T. (1966). Pore-and solid-diffusion kinetics in fixed-bed adsorption under constant-pattern conditions. *Industrial and Engineering Chemistry Fundamentals, 5*, 212–223.

He, F., & Zhao, D. (2005). Preparation and characterization of a new class of starch-stabilized bimetallic nanoparticles for degradation of chlorinated hydrocarbons in water. *Environmental Science & Technology, 39*, 3314–3320.

He, F., & Zhao, D. Y. (2007). Manipulating the size and dispersibility of zerovalent iron nanoparticles by use of carboxymethyl cellulose stabilizers. *Environmental Science & Technology, 41*, 6216–6221.

He, F., Zhao, D., Liu, J., & Roberts, C. B. (2007). Stabilization of Fe-Pd nanoparticles with sodium carboxymethyl cellulose for enhanced transport and dechlorination of trichloroethylene in soil and groundwater. *Industrial & Engineering Chemistry Research, 46*, 29–34.

Heidari, A., Younesi, H., & Mehraban, Z. (2009). Removal of Ni (II), Cd (II), and Pb (II) from a ternary aqueous solution by amino functionalized mesoporous and nano mesoporous silica. *Chemical Engineering Journal, 153*, 70–79.

Hou, M., Wan, H., Liu, T., Fan, Y., Liu, X., & Wang, X. (2008). The effect of different divalent cations on the reduction of hexavalent chromium by zerovalent iron. *Applied Catalysis B: Environmental, 84*, 170–175.

Hu, C. Y., Lo, S. L., Liou, Y. H., Hsu, Y. W., Shih, K., & Lin, C. J. (2010). Hexavalent chromium removal from near natural water by copper–iron bimetallic particles. *Water Research, 44*, 3101–3108.

Huang, D. L., Zeng, G. M., Jiang, X. Y., Feng, C. L., Yu, H. Y., Huang, G. H., & Liu, H. L. (2006). Bioremediation of Pb-contaminated soil by incubating with Phanerochaete chrysosporium and straw. *Journal of Hazardous Materials, 134*, 268–276.

Huang, D. L., Zeng, G. M., Feng, C. L., Hu, S., Jiang, X. Y., Tang, L., & Liu, H. L. (2008). Degradation of lead-contaminated lignocellulosic waste by phanerochaete chrysosporium and the reduction of lead toxicity. *Environmental Science & Technology, 42*, 4946–4951.

Iram, M., Guo, C., Guan, Y., Ishfaq, A., & Liu, H. (2010). Adsorption and magnetic removal of neutral red dye from aqueous solution using Fe_3O_4 hollow nanospheres. *Journal of Hazardous Materials, 181*, 1039–1050.

Jiang, W., Pelaez, M., Dionysiou, D. D., Entezari, M. H., Tsoutsou, D., & O'Shea, K. (2013). Chromium (VI) removal by maghemite nanoparticles. *Chemical Engineering Journal, 222*, 527–533.

Kanel, S. R., Greneche, J. M., & Choi, H. (2006). Arsenic(V) removal kom groundwater using nanoscale zero-valent iron as a colloidal reactive barrier material. *Environmental Science & Technology, 40*, 2045–2050.

Langmuir, I. (1916). The constitution and fundamental properties of solids and liquids. Part I Solids. *Journal of the American Chemical Society, 38*, 2221–2295.

Lee, T., Lim, H., Lee, Y., & Park, J. W. (2003). Use of waste iron metal for removal of Cr (VI) from water. *Chemosphere, 53*, 479–485.

Li, X. Q., & Zhang, W. X. (2006). Iron nanoparticles: the core–shell structure and unique properties for Ni(II) sequestration. *Langmuir, 22*, 4638–4642.

Li, L., Fan, M., Brown, R. C., Van Leeuwen, J., Wang, J., Wang, W., & Zhang, P. (2006). Synthesis, properties, and environmental applications of nanoscale iron-based materials: a review. *Critical Reviews in Environmental Science and Technology, 36*, 405–431.

Li, J., Lin, Q., Zhang, X., & Yan, Y. (2009). Kinetic parameters and mechanisms of the batch biosorption of Cr (VI) and Cr (III) onto Leersia hexandra Swartz biomass. *Journal of Colloid and Interface Science, 333*, 71–77.

Li, S., Wu, P., Li, H., Zhu, N., Li, P., Wu, J., & Dang, Z. (2010). Synthesis and characterization of organo-montmorillonite supported iron nanoparticles. *Applied Clay Science, 50*, 330–336.

Lin, S. H., & Juang, R. S. (2002). Heavy metal removal from water by sorption using surfactant-modified montmorillonite. *Journal of Hazardous Materials, 92*, 315–326.

NIH Washington D. C. (2007). NIH, NTP Technical report on the toxicity studies of sodium dichromate dihydrate

O'Carroll, D., Sleep, B., Krol, M., Boparai, H., & Kocur, C. (2013). Nanoscale zero valent iron and bimetallic particles for contaminated site remediation. *Advances in Water Resources, 51*, 104–122.

Phenrat, T., Saleh, N., Sirk, K., Tilton, R. D., & Lowry, G. V. (2007). Aggregation and sedimentation of aqueous nanoscale zerovalent iron dispersions. *Environmental Science & Technology, 41*, 284–290.

Powell, R. M., Puls, R. W., & Hightower, S. K. (1995). Coupled iron corrosion and chromate reduction: mechanisms for subsurface remediation. *Environmental Science & Technology, 29*, 1913–1922.

Reinsch, B. C., Forsberg, B., Penn, R. L., Kim, C. S., & Lowry, G. V. (2010). Chemical transformations during aging of zerovalent iron nanoparticles in the presence of common groundwater dissolved constituents. *Environmental Science & Technology, 44*, 3455–3461.

Rivero-Huguet, M., & Marshall, W. D. (2009a). Reduction of hexavalent chromium mediated by micro- and nano-sized mixed metallic particles. *Journal of Hazardous Materials, 169*, 1081–1087.

Rivero-Huguet, M., & Marshall, W. D. (2009b). Reduction of hexavalent chromium mediated by micron- and nano-scale zero-valent metallic particles. *Journal of Environmental Monitoring, 11*, 1072–1079.

Sun, Y. P., Li, X. Q., Cao, J., Zhang, W. X., & Wang, H. P. (2006). Characterization of zero-valent iron nanoparticles. *Advances in Colloid and Interface Science, 120*, 47–56.

Veintemillas-Verdaguer, S., Morales, M. P., & Serna, C. J. (1998). Continuous production of γ-Fe_2O_3 ultrafine powders by laser pyrolysis. *Materials Letters, 35*, 227–231.

Wang, C. T., & Ro, S. H. (2007). Nanoparticle iron–titanium oxide aerogels. *Materials Chemistry and Physics, 101*, 41–48.

Wang, Y., Fang, Z., Liang, B., & Tsang, E. P. (2014). Remediation of hexavalent chromium contaminated soil by stabilized nanoscale zero-valent iron prepared from steel pickling waste liquor. *Chemical Engineering Journal, 247*, 283–290.

White, B. R., Stackhouse, B. T., & Holcombe, J. A. (2009). Magnetic c-Fe_2O_3 nanoparticles coated with poly-L-cysteine for chelation of As(III), Cu(II), Cd(II), Ni(II), Pb(II) and Zn(II). *Journal of Hazardous Materials, 161*, 848–853.

Xu, P., Zeng, G. M., Huang, D. L., Lai, C., Zhao, M. H., Wei, Z., & Xie, G. X. (2012a). Adsorption of Pb (II) by iron oxide nanoparticles immobilized phanerochaete chrysosporium: equilibrium, kinetic, thermodynamic and mechanisms analysis. *Chemical Engineering Journal, 203*, 423–431.

Xu, P., Zeng, G. M., Huang, D. L., Feng, C. L., Hu, S., Zhao, M. H., & Liu, Z. F. (2012b). Use of iron oxide nanomaterials in wastewater treatment: a review. *Science of the Total Environment, 424*, 1–10.

Yin, K., Lo, I. M., Dong, H., Rao, P., & Mak, M. S. (2012). Lab-scale simulation of the fate and transport of nano zero-valent iron in subsurface environments: aggregation, sedimentation, and contaminant desorption. *Journal of Hazardous Materials, 227*, 118–125.

Yuan, P., Liu, D., Fan, M., Yang, D., Zhu, R., Ge, F., & He, H. (2010). Removal of hexavalent chromium [Cr(VI)] from aqueous solutions by the diatomite-supported/unsupported magnetite nanoparticles. *Journal of Hazardous Materials, 173*, 614–621.

Zhang, X. F., Yin, H. B., Cheng, X. N., Chen, K. M., Hu, H. F., Yu, Q., & Wang, A. L. (2006). Effects of Tweens and sodium dodecyl sulfate as modifiers on hydrothermal synthesis of nanocrystals copper. *Chinese Journal of Nonferrous Metals, 16*, 327.